

Observation of radiation pressure exerted by evanescent waves

D. Voigt, B. T. Wolschrijn, R. Jansen, N. Bhattacharya, R. J. C. Spreeuw,* and H. B. van Linden van den Heuvell
Van der Waals–Zeeman Institute, University of Amsterdam, Valckenierstraat 65, 1018 XE Amsterdam, the Netherlands

(Received 21 December 1999; published 16 May 2000)

We report a direct observation of radiation pressure, exerted on cold rubidium atoms while bouncing on an evanescent-wave atom mirror. We analyze the radiation pressure by imaging the motion of the atoms after the bounce. The number of absorbed photons is measured for laser detunings ranging from 190 MHz to 1.4 GHz and for angles from 0.9 mrad to 24 mrad above the critical angle of total internal reflection. Depending on these settings, we find velocity changes parallel with the mirror surface, ranging from 1 to 18 cm/s. This corresponds to 2 to 31 photon recoils per atom. These results are independent of the evanescent-wave optical power.

PACS number(s): 32.80.Lg, 42.50.Vk, 03.75.-b

I. INTRODUCTION

An evanescent wave (EW) appears whenever an electromagnetic wave undergoes total internal reflection at a dielectric interface. The EW is characterized by an electric field amplitude that decays exponentially with the distance to the interface. The decay length is on the order of the (reduced) optical wavelength. Cook and Hill [1] proposed to use the EW as a mirror for slow neutral atoms, based on the “dipole force.” EW mirrors have since become an important tool in atom optics [2]. They have been demonstrated for atomic beams at grazing incidence [3] and for ultracold atoms at normal incidence [4].

Most experimental work so far has been concentrated on the reflective properties, i.e., the change of the atomic motion *perpendicular* to the surface [5]. This is dominated by the dipole force due to the strong gradient of the electric field amplitude. In the present paper we report on our measurement of the force *parallel* to the surface. It was mentioned already in the original proposal [1] that there should be such a force. The propagating component of the wave vector leads to a spontaneous scattering force, “radiation pressure” [6,7]. We present here a direct observation of radiation pressure exerted by evanescent waves on cold atoms. Previously, a force parallel to the surface was observed for micrometer-sized dielectric spheres [8].

In our experiment, we observe the trajectory of a cloud of cold rubidium atoms falling and bouncing on a horizontal EW mirror. The radiation pressure appears as a change in horizontal velocity during the bounce. We study the average number of scattered photons per atom as a function of the detuning and angle of incidence of the EW. The latter varies the “steepness” of the optical potential.

Due to its short extension, on the order of the optical wavelength, an EW mirror is a promising tool for efficient loading of low-dimensional optical atom traps in the vicinity of the dielectric surface [9,10]. In these schemes, spontaneous optical transitions provide dissipation and cause the mirror to be “inelastic,” such that the final atomic phase-space density increases. This might open a route toward quantum degenerate gases that does not use evaporative cooling [11],

and could potentially yield “atom lasers” [12], which are open, driven systems out of thermal equilibrium, similar to optical lasers. It is this application of EW mirrors that drives our interest in experimental control of the photon scattering of bouncing atoms.

This article is structured as follows. In Sec. II we summarize the properties of the EW potential, including the photon scattering of a bouncing atom. In Sec. III we describe our experimental setup and our observation of radiation pressure. We investigate its dependence on the angle of incidence and laser detuning. Finally, we discuss several systematic errors.

II. THE EVANESCENT-WAVE ATOMIC MIRROR

A. Optical dipole potential

Our evanescent wave is created by total internal reflection at a glass surface in vacuum [13]. We choose the z direction as the surface normal and the xz plane as the plane of incidence (see Fig. 1). The EW can be written as $E(\mathbf{r}) \propto \exp(i\mathbf{k} \cdot \mathbf{r})$, where $\mathbf{k} = (k_x, 0, i\kappa)$. The wave vector has a propagating component along the surface, $k_x = k_0 n \sin \theta$, where $k_0 = 2\pi/\lambda_0$ is the vacuum wave number, n is the refractive index, and θ is the angle of incidence. Note that $k_x > k_0$, since θ is larger than the critical angle $\theta_c = \arcsin n^{-1}$. The wave vector component perpendicular to the surface is imaginary, with $\kappa = k_0 \sqrt{n^2 \sin^2 \theta - 1}$.

The optical dipole potential for a two-level atom at a distance z above the prism can then be written as $\mathcal{U}_{dip}(z) = \mathcal{U}_0 \exp(-2\kappa z)$. In the limit of large laser detuning $|\delta| \gg \Gamma$ and low saturation $s_0 \ll 1$, the maximum potential at the prism surface is $\mathcal{U}_0 = \hbar \delta s_0 / 2$, with a saturation parameter $s_0 \approx (\Gamma/2\delta)^2 T I / I_0$ [14]. Here, $I_0 = 1.65 \text{ mW/cm}^2$ is the saturation intensity for rubidium and $\Gamma = 2\pi \times 6.0 \text{ MHz}$ is the natural linewidth. The intensity of the incoming beam in the glass substrate is given as I . It is *enhanced* by a factor T , which ranges between 5.4 and 6.0 for our TM polarized EW [15]. The detuning of the laser frequency ω_L with respect to the atomic transition frequency ω_0 is defined as $\delta = \omega_L - \omega_0$. Thus a “blue” detuning, $\delta > 0$, yields an exponential potential barrier for incoming atoms. Given an incident atom with momentum p_i , a classical turning point of the motion

*Electronic address: spreeuw@wins.uva.nl

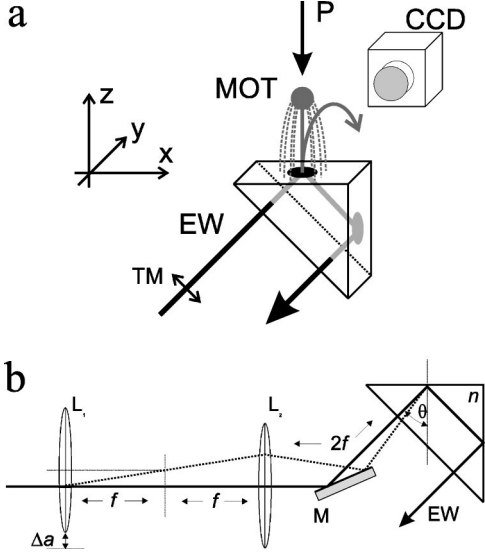


FIG. 1. Evanescent-wave atom mirror. (a) Configuration in the rubidium vapor cell: magneto-optical trap (MOT), right-angle prism with refractive index n (6.6 mm below the MOT, gravity $\parallel z$), evanescent-wave beam (EW), camera facing from the side (CCD, in y direction), resonant fluorescence probe beam from above (P). (b) Confocal relay telescope for adjusting the angle of incidence θ . The lenses $L_{1,2}$ have equal focal length, $f=75$ mm. A translation of L_1 by a distance Δa changes the angle of incidence by $\Delta\theta = \Delta a / fn$. The position of the EW spot remains fixed. M is a mirror.

exists if the barrier height exceeds the kinetic energy $p_i^2/2M$ of the atom.

For a purely optical potential, the barrier height is given by \mathcal{U}_0 . In reality, the potential is also influenced by gravity and the attractive van der Waals potential,

$$\mathcal{U} = \mathcal{U}_{dip} + \mathcal{U}_{grav} + \mathcal{U}_{vdW}. \quad (1)$$

The gravitational potential $\mathcal{U}_{grav}(z) \propto z$ can be neglected on the length scale of the EW decay length $\xi \equiv 1/\kappa$. The van der Waals potential $\mathcal{U}_{vdW}(z) \propto (k_0 z)^{-3}$ significantly lowers the maximum potential close to the prism and thus decreases the effective mirror surface on which atoms can still bounce. This effect has been demonstrated by Landragin *et al.* [16].

B. Photon scattering by bouncing atoms

The photon scattering rate of a two-level atom in steady state at low saturation can be written as $\Gamma' = s\Gamma/2 = (\Gamma/\hbar\delta)\mathcal{U}_{dip}$ [14]. An atom bouncing on an EW mirror sees a time-dependent saturation parameter $s(t)$. Assuming that the excited state population follows adiabatically, we can integrate the scattering rate along an atom's trajectory to get the number of scattered photons,

$$N_{scat} = \int \Gamma'(t) dt = \frac{\Gamma}{\hbar\delta} \int_{-p_i}^{+p_i} \left(\frac{\mathcal{U}_{dip}}{-\partial_z \mathcal{U}} \right) dp. \quad (2)$$

For a purely optical potential, $\mathcal{U} \propto \exp(-2\kappa z)$, this leads to an analytical solution:

$$N_{scat} = \frac{\Gamma}{\delta} \frac{p_i}{\hbar\kappa}. \quad (3)$$

The ‘‘steepness’’ of the optical potential is determined by κ . The steeper the potential, the shorter the time an atom spends in the light field, and the lower N_{scat} . Note that N_{scat} is independent of \mathcal{U}_0 , as a consequence of the $\exp(-2\kappa z)$ shape of the potential. This is in fact the reason why a two-level description of the atoms is appropriate. Strictly speaking, for a realistic atom the potential strength depends on the magnetic sublevel m_F through the Clebsch-Gordan coefficients. For example, our EW is TM polarized, which, close to the critical angle, is approximately linear. Effectively, for every m_F sublevel, \mathcal{U}_0 is then multiplied by the square of a Clebsch-Gordan coefficient, ranging from 1/3 to 3/5 (for an $F=2 \rightarrow F'=3$ transition). Remarkably though, the value of N_{scat} remains unaffected and the same for all atoms.

One expects that an absorbed photon will give a recoil momentum $p_{rec} = \hbar k_x$ to the atom, directed along the propagating component of the EW. Experimentally we observe this effect by the altered horizontal velocity of atom clouds after the bounce. The spontaneous emission of photons leads to heating of the cloud and thus to thermal expansion [17,18].

In principle, N_{scat} is changed if other than optical forces are present. For example, the van der Waals attraction tends to ‘‘soften’’ the potential and thus to increase N_{scat} . We investigated this numerically and found it to be negligible in our present experiment.

III. THE OBSERVATION OF RADIATION PRESSURE

A. Experimental setup

Our experiment is performed in a rubidium vapor cell. We trap about 10^7 atoms of ^{87}Rb in a magneto-optical trap (MOT) and subsequently cool them in optical molasses to 10 μK . The MOT is centered 6.6 mm above the horizontal surface of a right-angled BK7 prism ($n=1.51$, $\theta_c=41.4^\circ$ [19]), as shown in Fig. 1(a).

The EW beam emerges from a single-mode optical fiber and is collimated and directed to the prism through a relay telescope [see Fig. 1(b)]. The angle of incidence θ is controlled by the vertical displacement Δa of the first telescope lens L_1 . This lens directs the beam, whereas the second lens L_2 images it to a *fixed* spot at the prism surface. A displacement Δa leads to a variation in θ , given by $\Delta\theta = \Delta a / nf$. The focal length of both lenses is $f=75$ mm. The beam has a minimum waist of 335 μm at the surface ($1/e^2$ intensity radius). We checked the beam collimation and found it almost diffraction limited with a divergence half-angle of less than 1 mrad. We use TM polarization for the EW because it yields a stronger dipole potential than a TE polarized beam of the same power. Close to the critical angle, the ratio of potential heights is approximately n^2 [15].

For the EW, an injection-locked single-mode laser diode (Hitachi HL7851G98) provides us with up to 28 mW of optical power behind the fiber. It is seeded by an external-grating-stabilized diode laser, locked to the ^{87}Rb hyperfine

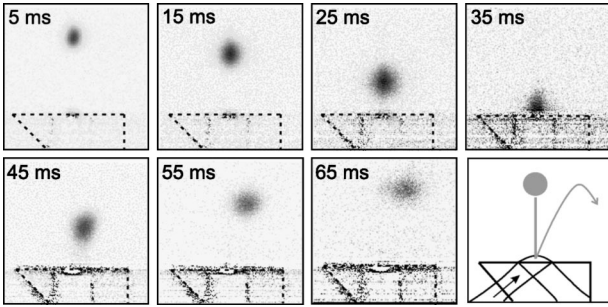


FIG. 2. Fluorescence images of a bouncing atom cloud. The first image was taken 5 ms after releasing the atoms from the MOT. The configuration of prism and evanescent wave is illustrated by the schematic (field of view: 10.2×10.2 mm²).

transition $5S_{1/2}(F=2) \rightarrow 5P_{3/2}(F'=3)$ of the D_2 line (780 nm), with a natural linewidth $\Gamma = 2\pi \times 6.0$ MHz. The detuning δ with respect to this transition defines the optical potential \mathcal{U}_{dip} for atoms that are released from the MOT in the $F=2$ ground state. We adjust detunings up to $2\pi \times 500$ MHz by frequency shifting the seed beam from resonance, using an acousto-optic modulator. For larger detunings we unlock the seed laser and set its frequency manually, according to the reading of an optical spectrum analyzer with 1 GHz free spectral range.

Atoms that have bounced on the EW mirror are detected by induced fluorescence from a pulsed probe beam, resonant with the $F=2 \rightarrow F'=3$ transition. The probe beam travels in the vertical downward direction and has a diameter of 10 mm. The fluorescence is recorded from the side, in the y direction, by a digital frame-transfer charge-coupled device (CCD) camera (Princeton Instruments). The integration time is chosen between 0.1 ms and 1 ms and is matched to the duration of the probe pulse. Each camera image consists of 400×400 pixels, that were hardware binned on the CCD chip in groups of four pixels. The field of view is 10.2×10.2 mm² with a spatial resolution of 51 μ m per pixel.

A typical timing sequence of the experiment is as follows. The MOT is loaded from the background vapor during 1 s. After 4 ms of polarization gradient cooling in optical molasses the atoms are released in the $F=2$ ground state by closing a shutter in the cooling laser beams. The image capture is triggered with a variable time delay after releasing the atoms. During the entire sequence, the EW laser is permanently on. In addition, a permanent repumping beam, tuned to the $5S_{1/2}(F=1) \rightarrow 5P_{1/2}(F'=2)$ transition of the D_1 line (795 nm), counteracts optical pumping to the $F=1$ ground state by the probe. We observed no significant influence on the performance of the EW mirror by the repumping light.

We measure the trajectories of bouncing atoms by taking a series of images with incremental time delays. A typical series with increments of 10 ms between the images is shown in Fig. 2. Our detection destroys the atom cloud, so a new sample was prepared for each image. The exposure time was 0.5 ms. Each image has been averaged over 10 shots. The fourth image shows the cloud just before the average bouncing time, $\bar{t}_b = 36.7$ ms, corresponding to the fall height of 6.6 mm. In later frames we see the atom cloud

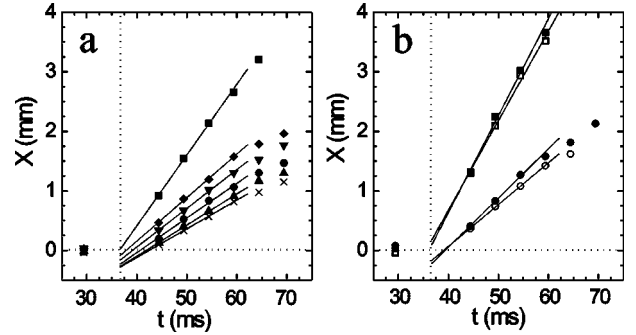


FIG. 3. Horizontal motion of bouncing atom clouds. The center of mass position is plotted vs time elapsed since release. The bounces occur at 36.7 ms (vertical dotted line). (a) The EW decay length is varied as $\xi(\theta) = 1.87, 1.03, 0.79, 0.67, 0.59, 0.53$ μ m (from large to small change in velocity). The detuning is 44Γ and the optical power is 19 mW. (b) Comparison of two values of EW optical power, 19 mW (solid points) and 10.5 mW (open points). The detuning is 31Γ and the EW decay lengths are $\xi = 1.87$ μ m (large velocity change) and 0.67 μ m (small change). Solid lines indicate linear fits.

bouncing up from the surface. Close to the prism, the fast vertical motion causes blurring of the image. Another cause of vertical blur is motion due to radiation pressure by the probe pulse. The horizontal motion of the clouds was not affected by the probe. We checked this by comparing with images taken with considerably shorter probe pulses of 0.1 ms duration.

B. Results

Radiation pressure in the evanescent wave was observed by analyzing the horizontal motion of the clouds. From the camera images we determine the center of mass position of the clouds to about ± 1 pixel accuracy. In Fig. 3, we plot the horizontal position vs time elapsed since release from the MOT. We find that the horizontal motion is uniform before and after the bounce. The horizontal velocity changes suddenly during the bounce as a consequence of scattering EW photons. The change in velocity is obtained from a linear fit.

In Fig. 4, we show how the radiation pressure depends on the laser detuning δ and on the angle of incidence θ . The fitted horizontal velocity change has been expressed in units of the EW photon recoil, $p_{rec} = \hbar k_0 n \sin \theta$, with $\hbar k_0 / M = 5.88$ mm/s.

In Fig. 4(a), the detuning is varied from 188 to 1400 MHz [$(31-233)\Gamma$]. Two sets of data are shown, taken for two different angles, $\theta = \theta_c + 0.9$ mrad and $\theta_c + 15.2$ mrad. This corresponds with EW decay lengths $\xi(\theta) = 2.8$ μ m and 0.67 μ m, respectively. We find that the number of scattered photons is inversely proportional to δ , as expected. The predictions based on Eq. (3) are indicated in the figure (solid lines).

In Fig. 4(b), the detuning was kept fixed at 44Γ and the angle of incidence was varied between 0.9 mrad and 24.0 mrad above the critical angle θ_c . This leads to a variation of $\xi(\theta)$ from 2.8 μ m to 0.53 μ m. Here also we find a linear dependence on $\xi(\theta)$. We see clearly that a steep optical po-

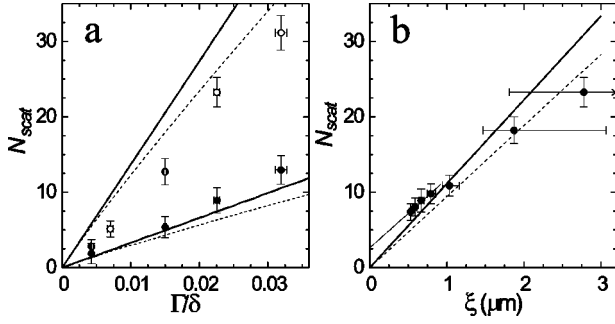


FIG. 4. Radiation pressure on bouncing atoms expressed as number of absorbed photons N_{scat} . (a) Detuning δ varied for $\xi = 2.8 \mu\text{m}$ (open points) and $0.67 \mu\text{m}$ (solid points). (b) EW decay length ξ varied for $\delta = 44\Gamma$. The laser power was 19 mW. The thin solid line is a linear fit through the first four data points. Theoretical predictions: two-level atom [see Eq. (3), thick solid lines]; rubidium excited state hyperfine structure and saturation taken into account (dashed lines).

tential, i.e., a small decay length, causes less radiation pressure than a shallow potential.

The observed radiation pressure ranges from 2 to 31 photon recoils per atom. Note that we separate this subtle effect from the faster vertical motion, in which atoms enter the optical potential with a momentum of $p_i \approx 61p_{rec}$.

In Fig. 3(b), we compare trajectories for 19 ± 1 mW and 10.5 ± 0.5 mW optical power in the EW. As expected from Eq. (3), there is no significant difference in horizontal motion. For a decay length of $\xi = 2.78 \mu\text{m}$ ($0.67 \mu\text{m}$) both power settings lead to essentially the same radiation pressure, that is, 25 ± 3 (13 ± 2) scattered photons for 19 mW, and 23 ± 2 (11 ± 1) photons for 10.5 mW. The optical power determines only the effective mirror surface and thus the fraction of bouncing atoms. This is also visible in the horizontal width of bouncing clouds. The bouncing fraction scales with the intensity and the detuning as $\propto \ln(I/\delta)$. We observe typical fractions of 13% for $\delta = 44\Gamma$. For a given optical power, there is an upper limit for the detuning, above which no bounce can occur. For the data in Fig. 4(a), the threshold is calculated as $\delta_{th} = 6.5$ GHz (8.1 GHz) for $\xi = 2.8 \mu\text{m}$ ($0.67 \mu\text{m}$). Another threshold condition is implied by the van der Waals interaction, and yields a lower limit for the EW decay length ξ . For Fig. 4(b) this lower limit is calculated as $\xi_{th} = 116$ nm, i.e., $\theta_{th} = (\theta_c + 0.59 \text{ rad})$.

C. Systematic errors and discussion

According to Eq. (3), the radiation pressure should be inversely proportional to both δ and $\kappa(\theta)$. As shown in Fig. 4, we find deviations from this expectation in our experiment, particularly in the κ dependence. A linear fit to the data for $\xi < 1 \mu\text{m}$ extrapolates to an offset of approximately three photon recoils in the limit $\xi \rightarrow 0$ [thin solid line in Fig. 4(b)]. The vertical error bars on the data include statistical errors in the velocity determination from the cloud trajectories as well as systematic errors. We discuss several possible systematic errors, namely, (i) the geometric alignment, (ii) the EW beam angle calibration and collimation, (iii) dif-

fusely scattered light, (iv) the van der Waals atom-surface interaction, (v) excited state contributions to the optical potential, and (vi) saturation effects.

(i) Geometrical misalignments give rise to systematic errors in the radiation pressure measurements. For example, a tilt of the prism causes a horizontal velocity change even for specularly reflected atoms. We checked the prism alignment and found it tilted 12 ± 5 mrad from horizontal. This corresponds to an offset of 1.5 ± 0.6 recoils on N_{scat} . In addition, the atoms are ‘‘launched’’ from the MOT with a small initial horizontal velocity which we found to correspond to less than ± 0.4 recoils for all our data. From Fig. 3, we see that the extrapolated trajectories at the bouncing time \bar{t}_b do not start from the horizontal position before the bounce. We attribute this to a horizontal misalignment of the MOT with respect to the EW spot. Obviously, there is a small displacement of the EW spot at the prism surface, when adjusting θ by means of the lens L_1 [see Fig. 1(b)]. Since the finite-sized EW mirror reflects only part of the thermally expanding atom cloud, such a displacement selects a nonzero horizontal velocity for bouncing atoms. We corrected for those alignment effects in the radiation pressure data of Fig. 4. For small radiation pressure values, the systematic error due to alignment is the dominant contribution in the vertical error bar.

(ii) The uncertainty in the EW angle with respect to the critical angle is expressed by the horizontal error bars. We determined $\theta - \theta_c$ within ± 0.2 mrad by monitoring the optical power transmitted through the prism surface, while tuning the angle θ from below to above θ_c . Close to the critical angle, the decay length $\xi(\theta)$ diverges, and thus the error bar on ξ becomes very large. Also, the diffraction-limited divergence of the EW beam may become significant. It causes part of the optical power to propagate into the vacuum. In addition, the optical potential is governed by a whole distribution of decay lengths. Thus the model of a simple exponential optical potential proportional to $\exp(-2\kappa z)$ might not be valid, which would cause the disagreement of our data with the prediction of Eq. (3). For larger angles, i.e., $\xi(\theta) < 1 \mu\text{m}$, the effect of the beam divergence is negligible. This we could verify by numerical analysis.

(iii) Light from the EW can diffusely scatter and propagate into the vacuum due to roughness of the prism surface. We presume this is the reason for the extrapolated offset of three photon recoils in the radiation pressure [Fig. 4(b)]. A preferential light scattering in the direction of the EW propagating component can be explained if the power spectrum of the surface roughness is narrow compared to $1/\lambda$ [18]. The effect of surface roughness on bouncing atoms has previously been observed [17] as a broadening of atom clouds by the roughness of the *dipole potential*. In our case, we observe a change in center of mass motion of the clouds due to an increase in the *spontaneous scattering force*. Such a contribution to the radiation pressure due to surface roughness vanishes in the limit of large detuning δ . Thus, we find no significant offset in Fig. 4(a). Scattered light might also be the reason for the small difference in radiation pressure for the two distinct EW power settings shown in Fig. 3(b).

Lower optical power implies slightly less radiation pressure.

(iv) As stated above, the van der Waals interaction “softens” the mirror potential. This makes bouncing atoms move longer in the light field, thus enhancing photon scattering. We investigated this numerically by integrating the scattering rate along the atoms’ path, including the van der Waals contribution to the mirror potential. Even for our shortest decay parameter of $0.53 \mu\text{m}$, the number of scattered photons would increase only about 0.8% compared with Eq. (3), which we cannot resolve experimentally [20].

(v) In a two-level atom model, the scattering rate can be expressed in the dipole potential as $\Gamma' = (\Gamma/\hbar\delta)\mathcal{U}_{dip}$. This is no longer true if we take into account the excited state manifold $F' = \{0,1,2,3\}$ of ^{87}Rb . In addition to $F' = 3$, $F' = 2$ also contributes significantly to the mirror potential, whereas it does not much affect the scattering rate. With an EW detuning of 44Γ , this results in a number of scattered photons N_{scat} typically 9% lower than expected for a two-level atom, Eq. (3). Here we averaged over contributions from distinct magnetic sublevels.

(vi) In order to investigate the influence of saturation on the number of scattered photons N_{scat} , we solved the optical Bloch equations numerically. A bouncing atom encounters the EW as a fast varying light pulse $I(t) \propto \text{sech}^2(\kappa p_i t/M)$, with a typical duration between 3 and 10 μs . By integrating the time-dependent scattering rate for an atom bouncing with an EW detuning of 44Γ , we find approximately 7% fewer scattered photons compared with the unsaturated expression of Eq. (3). Note that the bounces occur sufficiently slowly to preserve adiabaticity. In Fig. 4, we show predicted curves, corrected for hyperfine structure and saturation (dashed solid lines).

IV. CONCLUSIONS

We have directly observed radiation pressure that is exerted on rubidium atoms while bouncing on an evanescent-

wave atom mirror. We did so by analyzing the bouncing trajectories. The radiation pressure is directed parallel to the propagating component of the EW, i.e., parallel to the interface. We observe 2 to 31 photon recoils per atom per bounce. We find the radiation pressure to be independent of the optical power in the EW, as expected from the exponential character of the EW.

The inverse proportionality to both the EW detuning and the angle of incidence is in reasonable agreement with a simple two-level atom calculation, using steady state expressions for the EW optical potential and the photon scattering rate. The agreement improved when the excited state hyperfine structure and saturation effects were also taken into account. The measured number of photon recoils as a function of decay length ξ indicates an offset of approximately 3 recoils in the limit of a very steep EW potential. We assume this is due to light that is diffusely scattered because of roughness of the prism surface, but retains a preferential forward direction parallel with the EW propagating component.

With sufficient resolution, it should be possible to resolve the discrete nature of the number of photon recoils and also their magnitude, $\hbar k_x > \hbar k_0$. Our technique could also be used to observe quantum electrodynamical effects for atoms in the vicinity of a surface, such as radiation pressure out of the direction of the propagating EW component [21].

ACKNOWLEDGMENTS

We wish to thank E. C. Schilder for help with the experiments. This work is part of the research program of the “Stichting voor Fundamenteel Onderzoek van de Materie” (Foundation for the Fundamental Research on Matter) and was made possible by financial support from the “Nederlandse Organisatie voor Wetenschappelijk Onderzoek” (Netherlands Organization for the Advancement of Research). R.S. has been financially supported by the Royal Netherlands Academy of Arts and Sciences.

-
- [1] R. J. Cook and R. K. Hill, *Opt. Commun.* **43**, 258 (1982).
 [2] C. S. Adams, M. Sigel, and J. Mlynek, *Phys. Rep.* **240**, 143 (1994).
 [3] V. I. Balykin, V. S. Letokhov, Yu. B. Ovchinnikov, and A. I. Sidorov, *Pis'ma Zh. Éksp. Teor. Fiz.* **45**, 282 (1987) [*JETP Lett.* **45**, 353 (1987)].
 [4] M. A. Kasevich, D. S. Weiss, and S. Chu, *Opt. Lett.* **15**, 607 (1990).
 [5] W. Seifert, C. S. Adams, V. I. Balykin, C. Heine, Yu. Ovchinnikov, and J. Mlynek, *Phys. Rev. A* **49**, 3814 (1994).
 [6] J. P. Gordon and A. Ashkin, *Phys. Rev. A* **21**, 1606 (1980).
 [7] R. J. Cook, *Phys. Rev. A* **22**, 1078 (1980).
 [8] S. Kawata and T. Sugiura, *Opt. Lett.* **17**, 772 (1992).
 [9] Yu. B. Ovchinnikov, S. V. Shul'ga, and V. I. Balykin, *J. Phys. B* **24**, 3173 (1991); P. Desbiolles and J. Dalibard, *Opt. Commun.* **132**, 540 (1996); Yu. B. Ovchinnikov, I. Manek, and R. Grimm, *Phys. Rev. Lett.* **79**, 2225 (1997); W. L. Power, T. Pfau, and M. Wilkens, *Opt. Commun.* **143**, 125 (1997); H. Gauck, M. Hartl, D. Schneble, H. Schnitzler, T. Pfau, and J. Mlynek, *Phys. Rev. Lett.* **81**, 5298 (1998).
 [10] R. J. C. Spreeuw, D. Voigt, B. T. Wolschrijn, and H. B. van Linden van den Heuvell, e-print quant-ph/9911017.
 [11] For a recent review on Bose-Einstein condensation, see W. Ketterle, D. S. Durfee, and D. M. Stamper-Kurn, in *Bose-Einstein Condensation in Atomic Gases*, Proceedings of the International School of Physics “Enrico Fermi,” Course CXL, edited by M. Inguscio, S. Stringari, and C. Wieman (IOS Press, Amsterdam, 1999).
 [12] M.-O. Mewes, M. R. Andrews, D. M. Kurn, D. S. Durfee, C. G. Townsend, and W. Ketterle, *Phys. Rev. Lett.* **78**, 582 (1997); B. P. Anderson and M. A. Kasevich, *Science* **282**, 1686 (1998); E. Hagley, L. Deng, M. Kozuma, J. Wen, K. Helmerson, S. L. Rolston, and W. D. Phillips, *ibid.* **283**, 1706 (1999); I. Bloch, T. W. Hänsch, and T. Esslinger, *Phys. Rev. Lett.* **82**, 3008 (1999).
 [13] E. Hecht, *Optics* (Addison-Wesley, Reading, MA, 1987).
 [14] C. N. Cohen-Tannoudji, J. Dupont-Roc, and G. Grynberg, *Atom-Photon Interactions* (Wiley, New York, 1992).

- [15] The enhancement factor of the EW “intensity” is calculated for TM and TE polarization as $T_{\text{TM}}=4n \cos^2 \theta(2n^2 \sin^2 \theta - 1)/[\cos^2 \theta + n^2(n^2 \sin^2 \theta - 1)]$ and $T_{\text{TE}}=4n \cos^2 \theta/(n^2 - 1)$.
- [16] A. Landragin, J.-Y. Courtois, G. Labeyrie, N. Vansteenkiste, C. I. Westbrook, and A. Aspect, Phys. Rev. Lett. **77**, 1464 (1996).
- [17] A. Landragin, G. Labeyrie, C. Henkel, R. Kaiser, N. Vansteenkiste, C. I. Westbrook, and A. Aspect, Opt. Lett. **21**, 1591 (1996).
- [18] C. Henkel, K. Mølmer, R. Kaiser, N. Vansteenkiste, C. I. Westbrook, and A. Aspect, Phys. Rev. A **55**, 1160 (1997).
- [19] Melles Griot, high precision prism, order no. 01 PRB 009. We have cut it to a size of $10 \times 10 \times 4$ mm³.
- [20] As an example where van der Waals interaction is significant, for $\delta=1$ GHz, $\xi=370$ nm, and 2.5 mW optical power, the calculated number of scattered photons per bounce increases from 1.09 to 1.13 due to the van der Waals interaction.
- [21] C. Henkel and J.-Y. Courtois, Eur. Phys. J. D **3**, 129 (1998).